

# Hund's coupling mediated colossal increment in $T_c$ in multi-band FeSe manifold

Swagata Acharya, Francois Jamet, Dimitar Pashov, and Mark van Schilfgaarde

King's College London, Theory and Simulation of Condensed Matter, The Strand, WC2R 2LS London, UK\*

The normal phase of many unconventional superconductors is a “bad metal,” identified by incoherence in the quasi-particle spectrum, among other features. Hund's correlation has been identified as one strong source of bad metallicity in multi-band superconducting manifold. Using FeSe as a representative Hund's metal, we show that the superconducting critical temperature  $T_c$  is controlled by incoherence. In FeSe it is the  $d_{xy}$  orbital which becomes strongly incoherent, in presence of Hund's coupling  $J$ , when it is proximate to the Fermi level. Small excursions in  $J$  cause colossal changes in  $T_c$ . By applying a recently developed, high-fidelity *ab initio* theory as a starting reference to crystalline FeSe, we consider various kinds excursions in parameter space around the *ab initio* values, to determine what controls  $T_c$ . In addition to tuning  $J$  we consider doping, and structural changes by varying the Se position in both bulk and monolayer variants of FeSe. The twin combination of proximity of the  $d_{xy}$  state to the Fermi energy, and the strength of  $J$  emerge as the primary criterion for incoherent spectral response that in turn controls  $T_c$ . Using constrained RPA we show that experimentally accessible techniques can modify  $J$  by of order 100 meV, and give rise to dramatic changes in  $T_c$ . Our study, effectively, opens a paradigm for a unified understanding what controls  $T_c$  in bulk, layers, and interfaces of Hund's metals by hole pocket and electron screening cloud engineering.

Realizing superconductors at a practicable temperature has been one of the ‘holy grails’ of modern day materials research. Most conventional superconductors, governed by the BCS mechanism of Cooper pairing mediated by electron-phonon coupling, are found to have low superconducting critical temperature  $T_c$ . Stronger electronic correlations observed in most cuprates and iron-based superconductors have, more often than not, realized higher  $T_c$ 's. This has posed an interesting question: is strong electronic correlations prerequisite for higher  $T_c$ 's<sup>1,2</sup>? However, strong electronic correlations manifest itself in several forms: Mott-insulating states, bad metals and quantum critical scaling features are some among many. While  $T_c$  maximizes far from the Mott state in cuprates, in iron arsenides<sup>3</sup> and some f-electron based systems<sup>4-6</sup>,  $T_c$  maximizes in the proximity of a Mott state. On the other hand in almost all cuprates and iron based superconductors there appears a ‘bad metal’ phase<sup>7-16</sup> which is normal to the superconducting phase. Interestingly, this bad metallic phase is absent from the normal phase of all electron-phonon coupling mediated conventional superconductors. This ‘bad metal’ is a metallic phase characterized by unusually low quasi-particle weight, large single-particle scattering rates, poor and anomalous electron transport. Understanding the microscopic origin of such bad metallic behavior, hence, is at the core of investigation into the ‘universal’ precursors to the unconventional high- $T_c$  superconductivity. One primary conclusion of this paper is that incoherent spin fluctuations, controlled by Hund's coupling, in the vicinity of an antiferromagnetic ordering vector are the prime controlling element that governs  $T_c$  in several variants of FeSe.

In recent years, Hund's coupling have been shown to play an important role in controlling bad metallic features<sup>17,18</sup>, for example through small departures from the half-filled Mott limit ( $d^1, d^5, d^9$  configurations), which

can lead to strong electronic correlations<sup>17,19,20</sup>. In particular, it plays an important role in controlling single- and two-particle spectral properties of  $\text{Sr}_2\text{RuO}_4$ <sup>21-24</sup> in the normal phase.  $\text{Sr}_2\text{RuO}_4$ , with a modest  $T_c$  of 1.45 K under ambient conditions (reaching 3.4 K under uniaxial strain), has a 3-band manifold near the Fermi level  $E_F$  comprised of  $t_{2g}$  like states. It is in a  $4d^4$  electronic configuration, well away from the Mott limit (both in its filling and  $d$  bandwidth). It has a bad metallic phase for  $T > T_{FL}=25\text{ K}$ <sup>25-28</sup>; incoherence seems to be connected with a large continuum of background fluctuations with a sharp peak in the vicinity of  $k$  points  $(\pm 0.3, \pm 0.3)2\pi/a$  in the 2D Brillouin zone<sup>21,24</sup>.

FeSe is also far from the half-filled Mott limit with a  $3d^6$  electronic configuration and all five  $d$  states active near  $E_F$ , but with spin-orbit coupling smaller than its  $4d$  counterparts. There is a phase transition to the orthorhombic phase at 90 K<sup>29</sup>. Spin fluctuations are concentrated in a region around the antiferromagnetic point, which is  $(1/2, 1/2)2\pi/a$  in the Brillouin of the two Fe-atom unit cell (which is  $(1, 0)$  in one fe-atom unit cell); though there is a smaller contribution at  $(1/2, 0)$ . Experimentally, “Hundness” has been found to highly orbital selective in FeSe.<sup>30</sup> Superconductivity is widely thought to be spin singlet character, likely of  $s\pm$ <sup>31,32</sup>. In bulk FeSe  $T_c=9\text{ K}$ , but it can increase up to 75 K when deposited as a monolayer  $\text{SrTiO}_3$ <sup>33</sup>, and 109 K on doped  $\text{SrTiO}_3$ .<sup>34</sup> Thus while “Hundness” has been found to be important in controlling the single- and two-particle spectral properties of FeSe<sup>30,35,36</sup>, the multiplicity of factors (orbital character, spin-orbit coupling, shape of Fermi surface and dispersion of states around it, differences in susceptibilities that drive superconductivity, nematicity) obfuscate to what extent Hundness, or other factors, drive superconductivity.

In this work we isolate the effect of “Hundness” by making excursions in the Hund's parameter  $J$  as a free

parameter. We further show, using constrained RPA, that  $J$  can be tuned by varying the screening through, e.g. changes in the geometry such as the change from bulk to monolayer. We also show that while Hundness plays a central role, it alone does not control  $T_c$ . For FeSe in particular, we show that Hundness primarily affects the  $d_{xy}$  orbital, and that in addition to  $J$  the position of this orbital is crucial in governing  $T_c$ .

We begin with a high fidelity *ab initio* Hamiltonian, which merges quasiparticle self consistent  $GW$  (QSGW) approximation<sup>37</sup> with dynamical mean field theory (DMFT)<sup>21,38,39</sup>. The latter is solved for all five Fe-3d orbitals using a Continuous time Quantum Monte Carlo technique (CTQMC) on a rotationally invariant Coulomb interaction. QSGW captures non-local dynamic correlation particularly well in the charge channel<sup>40,41</sup>, but cannot adequately capture effects of spin fluctuations. DMFT does an excellent job at the latter, which are strong but mostly controlled by a local effective interaction given by  $U$  and  $J$ . These are calculated within the constrained RPA from the QSGW Hamiltonian using an approach similar to that of Ref.<sup>42</sup>.

Given a self-energy generated by QSGW+DMFT, spin and charge susceptibilities are obtained via the solutions of non-local Bethe Salpeter equation that links the local vertex (computed from the two-particle Green's function by DMFT) and nonlocal bubble diagrams. The numerical implementation is discussed in Pashov et. al.<sup>41</sup> and codes are available on the open source electron structure suite Questaal<sup>43</sup>. Additionally we compute the particle-particle vertex functions and solve the linearized Eliashberg equation<sup>21,44,45</sup> to compute the superconducting susceptibilities and eigenvalues of superconducting gap instabilities. QSGW+DMFT+BSE reproduces the main features of neutron structure factor<sup>46,47</sup>. Starting from the observed structure and *ab initio* Hamiltonian as a reference,

For the crystal, we find  $U=3.4$  eV and  $J=0.6$  eV from c-RPA calculated using the QSGW band structure. To assess the role of ‘‘Hundness’’ we perform a family of calculations making excursion in  $J$  between 0 and 1 eV. The single-particle scattering rate, obtained from low energy fitting analysis<sup>23,49</sup> of imaginary part of the self energy on the Matsubara axis (explained in SM), is found to be insensitive to  $J$  for  $J < 0.4$  eV. For  $J$  between 0.4 and 0.7 eV, it increases almost monotonically. At the same time the quasi-particle weight ( $Z$  factor) which is 0.75 for  $J=0$ , decreases with  $J$  up to  $J\sim 0.68$  eV reaching a minimum value of 0.24 (see SM, for Fig. 5 for  $J$  dependence of orbitally resolved  $Z$  and scattering rate  $\Gamma$ ) there, and then increases weakly for larger  $J$ . Thus there is smooth transition from coherent to increasingly incoherence with increasing  $J$ . A similar non-monotonic behavior was observed in previous studies of Hund’s metals<sup>50</sup>. Also  $Z$  is found to be strongly orbital selective. For  $J < 0.6$  eV, it is smallest for  $d_{xy}$ <sup>36</sup>, followed by  $d_{yz}$ ,  $d_{z^2}$  and  $d_{x^2-y^2}$  in increasing order<sup>51</sup>. Also we find the scattering rate to be largest for  $d_{xy}$ , followed by  $d_{yz}$ ,

$d_{z^2}$  and  $d_{x^2-y^2}$ . Similar conclusions were drawn in a recent orbitally resolved quasi-particle scattering interference measurements performed by Kostin et al.<sup>30</sup> in the low temperature orthorhombic phase of FeSe. Crucially, for  $J$  in the 0.6-0.7 eV range where the superconducting instability is strongest,  $d_{yz}$  is the orbital is most incoherent. The spectral functions shown in Fig. 1 show the enhanced incoherence due to increased  $J$ . At the point where  $T_c$  maximizes ( $J=0.68$  eV) the heaviest electron with most incoherent single-particle scattering resides in  $d_{xy}$ .

One crucial effect of  $J$  is to induce strong correlations: heavy and incoherent quasi-particles emerge with suppressed dispersion in the bands, which gives rise to marked changes in the spin susceptibility. Fig. 2 shows  $\text{Im} \chi(q, \omega)$  along the  $(0,0) \rightarrow (1/2,0) \rightarrow (1/2,1/2)$  lines (notation is for the true Fe<sub>2</sub>Se<sub>2</sub> unit cell with  $q_z=0$ ). Increasing  $J$  causes  $\text{Im} \chi(q, \omega)$  to be significantly compressed in energy, and the peak near  $(1/2,1/2)$  becomes more intense. It nevertheless continues to be broad in both momentum and energy, which suppresses the tendency towards magnetic ordering<sup>46,47,52</sup>. With further increment in  $J$  the  $(1/2,1/2)$  peak loses intensity. Resolving  $\text{Im} \chi$  into orbital channels,  $d_{xy}$  is seen to be the leading component. On the  $(0,0) \rightarrow (1/2,0)$  it contributing about 50% of the total with  $d_{z^2}$ ,  $d_{x^2-y^2}$  and  $d_{xz,yz}$  combining to contribute the rest. More importantly, along the path  $(1/2,0) \rightarrow (1/2,1/2)$  more than 90% of  $\text{Im} \chi$  originates from  $d_{xy}$ .

How do these striking changes in  $\text{Im} \chi$  correlate with  $T_c$ ? The eigenvalues and eigenfunctions of superconducting susceptibilities, superconducting pairing symmetries can not be extracted from the spin dynamics alone. We compute the full two particle scattering amplitude in the particle-particle channel within our DMFT framework, and solve Eliashberg equations in the BCS low energy approximation<sup>21,44,45</sup>. Resolving the eigenfunctions of the gap equation, into different inter- and intra-orbital channels, we find that there are two dominant eigenvalues. Both eigenvalues increase with  $J$  up to  $J=0.68$  eV, and then decrease (see SM). The corresponding eigenfunctions have extended  $s\pm$  wave character (leading eigenvalue) and  $d_{x^2-y^2}$  (second eigenvalue); see Fig. 3. We also find that these instabilities are primarily in the intra-orbital  $d_{xy}$ - $d_{xy}$  channel and the inter-orbital components are negligible.  $T_c$  reaches its maximum value (104 K) in the bulk crystal at  $J=0.68$  eV. At still larger  $J$ ,  $T_c$  begins to fall again, correlating with softening of electron masses and loss of spin fluctuations at  $q = (1/2, 1/2)$  (see Fig. 5 in SM).

We next investigate the effect changes to the spectral function,  $\chi$  and  $T_c$  induced by parametric changes in the one-body Hamiltonian. We first vary the Fe-Se bond length on  $T_c$ , which is typically parameterized by the height  $h_{Se}$  of Se above the Fe basal plane. As  $h_{Se}$  is reduced from its experimental value (0.2655 in units of the  $c$  axis), we find band of primarily  $d_{xy}$  character at the  $\Gamma$  point, and which crosses  $E_F$  is pushed down.

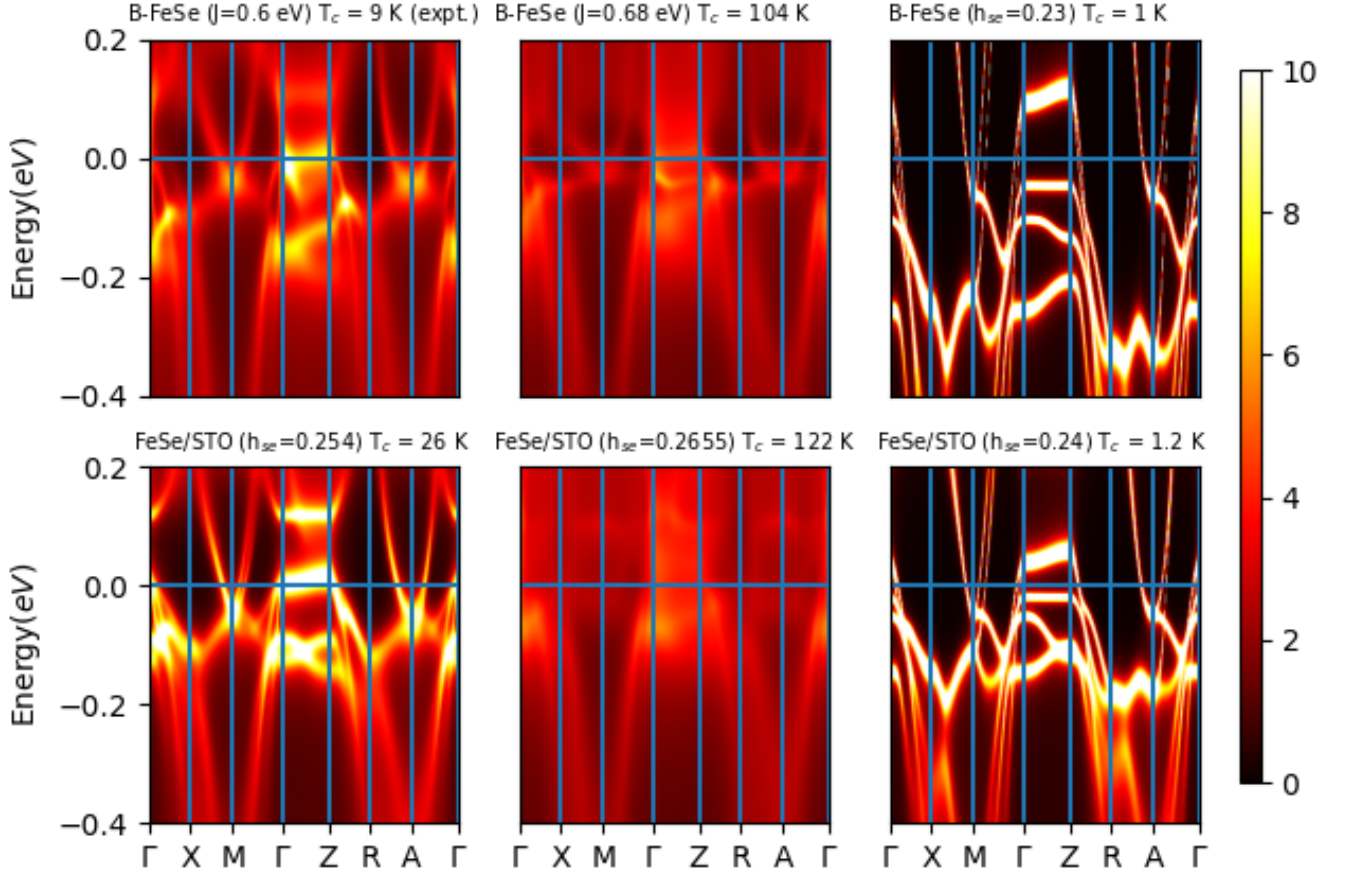


FIG. 1. Spectral function  $A(k, \omega)$  in FeSe. Top panel left to right : bulk FeSe, B-FeSe ( $J=0.6$  eV); same with Hund's coupling increased to  $0.68$  eV; same with reduced Se height above the Fe plane ( $h_{Se}=0.23$ ). Bottom panel: monolayer of FeSe to simulate FeSe/STO<sup>48</sup>. Left to right:  $h_{Se}=0.254$ ;  $h_{Se}=0.2655$ ;  $h_{Se}=0.24$ . The position of the Fe  $d_{xy}$  state is very sensitive to  $h_{Se}$ : when it is fixed to bring  $d_{xy}$  state near the Fermi energy, this leads to enhanced incoherence in the spectral features and higher superconducting  $T_c$ . The incoherence is further tuned by Hund's coupling;  $T_c$  at an optimum combination of the two lower chalcogen height in both bulk and monolayer FeSe/STO the Fe- $d_{xy}$  state is pushed below the Fermi energy at  $\Gamma$  point, leads to coherent spectral features and lowered  $T_c$ .

It is particularly easy to see at the QSGW level (see blue band in SM, Fig. 4), reaching about  $E_F - 160$  meV when  $h_{Se}=0.23$ . From c-RPA we compute the corresponding  $U$  and  $J$ :  $3.9$  eV and  $0.71$  eV respectively. A similar shift is found in the spectral function calculated by QSGW+DMFT (Fig. 1). Further, the change in  $h_{Se}$  causes quasi-particles to become coherent with orbital selective quasi-particle weights ranging between  $0.6$  to  $0.75$ . Scattering rates become weaker as well ( $20$ - $40$  meV). Thus the system appears to be a good metal. The peak in  $\text{Im}\chi(q, \omega)$  at  $(1/2, 1/2)$  shifts to higher  $\omega$  and becomes very weak (Fig. 2). Eigenvalues of the Eliashberg equations become negligibly small, suggesting extremely weak or no superconducting instability:  $T_c$  is estimated to be on the order of  $1$  K, and moreover it becomes com-

pletely insensitive to  $J$ .

That the  $d_{xy}$  orbital controls the transition from bad-metal, superconductor to good metal without superconductivity can be seen by parameterizing the QSGW Hamiltonian around its *ab initio* point in carefully controlled manner that targets the  $d_{xy}$  orbitals. We add an artificial Hubbard  $U$  to the QSGW Hamiltonian, on the Fe  $3d$  states. We use an artificial density matrix  $n$  that shifts only the potential on the  $d_{xy}$  partial wave. To compensate for the shift in  $E_F$  caused by  $d_{xy}$  shifting down, we simultaneously adding a uniform background charge  $Q$ . The net effect is to shift states of  $d_{xy}$  character while leaving all of the other states nearly unchanged. We performed this parameterization for two sets of  $(n, U, Q)$ : the first inducing a shift  $\Delta V = nU = -0.1$  eV, compen-

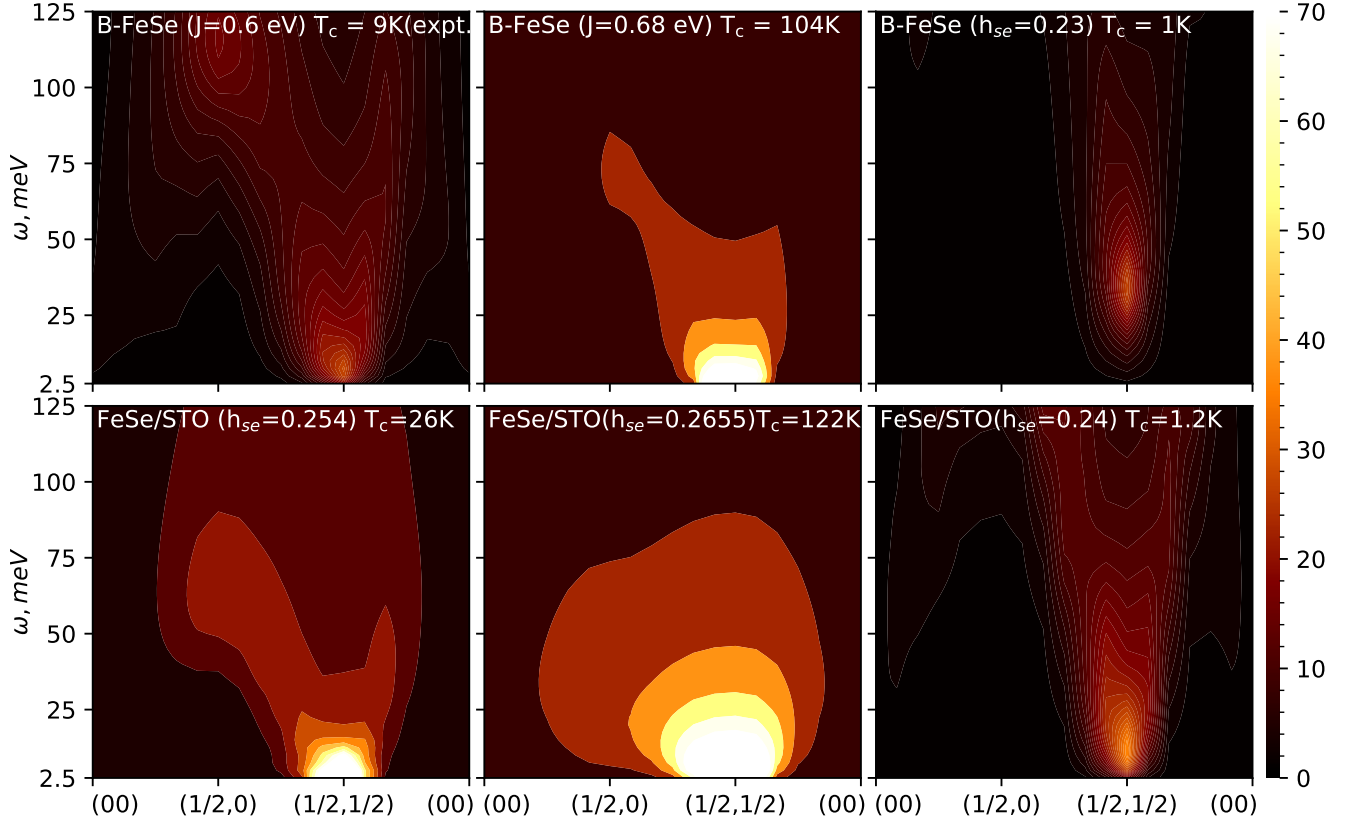


FIG. 2. The energy and momentum resolved spin susceptibility  $\text{Im}\chi(q, \omega)$  (in the top panel from left to right) shown for bulk FeSe (B-FeSe) ( $J=0.6$  eV), bulk FeSe with increased Hund's correlation ( $J=0.68$  eV), and reduced Fe-Se height ( $h_{se}=0.23$ ).  $\text{Im}\chi(q, \omega)$  (in the bottom panel from left to right) for FeSe/STO<sup>48</sup>, FeSe/STO with  $h_{se} = 0.2655$  and  $h_{se} = 0.24$ . The  $q$ -path (H,K,L=0) chosen is along  $(0,0)-(\frac{1}{2}, 0)-(\frac{1}{2}, \frac{1}{2})-(0,0)$  in the Brillouin zone corresponding to the two Fe-atom unit cell. The intensity of the spin fluctuations at  $(\frac{1}{2}, \frac{1}{2})$  is directly related to the presence of the Fe- $d_{xy}$  state at Fermi energy and its incoherence. The more incoherent the  $A(k, \omega)$  is the more intense is the  $\text{Im}\chi(q = (\frac{1}{2}, \frac{1}{2}), \omega)$ .

sated by  $0.155e$  background charge, the second shifting  $d_{xy}$  by  $\Delta V = nU = -0.2$  eV, compensated with  $0.211e$  background charge. The QP band structures are remarkably similar to the *ab initio* case, apart from the shift in the  $d_{xy}$  band (compare band bottom panels in SM, Fig. 4, to top left panel). Changes to the QSGW+DMFT spectral function, susceptibility and Eliashberg eigenvalues are very similar to those caused by changes in  $h_{se}$ : the spectral function becomes more coherent, the intensity of  $\text{Im}\chi(q, \omega)$  at  $(1/2, 1/2)$  becomes weak and  $T_c$  becomes very small.

These two parametric studies establish that for crystalline FeSe,  $T_c$  is controlled by two key parameters. For  $T_c$  to be high, the  $d_{xy}$  state must be close to, or crossing  $E_F$ . Once this favorable band structure emerges, large Hund's coupling can strongly enhance the incoherence and subsequently confine spin fluctuations to low energies and enhance the intensity in the vicinity of the antiferromagnetic  $q$  vector.

We finally turn to a monolayer of FeSe on STO. We take the structural inputs from a recent study by Mondal et al.<sup>48</sup> which finds the minimum-energy value for

$h_{se}$  within a combined DFT+DMFT framework. As a benchmark, that work found for bulk crystalline FeSe, the equilibrium  $h_{se}$  to be close to the measured value<sup>53</sup> (while DFT underestimates it). The same theory applied to FeSe/STO predicts  $h_{se}$  shrinks to 0.254 (DFT also predicts  $\delta h_{se} < 0$ ).

A QSGW calculation for the monolayer at  $h_{se}=0.254$  shows that the  $d_{xy}$  band is pushed down to  $E_F - 30$  meV on the  $\Gamma$ -Z line (Fig. 4 in SM, left middle panel). By performing c-RPA we obtain  $U=3.6$  eV and  $J=0.68$  eV. Moving to QSGW+DMFT, small and orbital dependent  $Z$  factors (0.28, 0.34, 0.31, 0.39 on  $xy$ ,  $z^2$ ,  $yz+xz$ ,  $x^2-y^2$ ) are extracted from similar analysis performed in the crystalline case, and the scattering rate continues to be largest on  $d_{xy}$ .  $\text{Im}\chi(q, \omega)$  continues to be dominated by fluctuations in the  $d_{xy}$  channel.  $(1/2, 1/2)$  is still the most intense peak (more intense than the bulk). That the dispersion in  $\text{Im}\chi(q, \omega)$  is narrowed, and intensity at  $(1/2, 1/2)$  concentrated at small  $\omega$ , suggest that FeSe/STO is more correlated than the bulk. Also of the two leading eigenvalues of the Eliashberg equation, the (dominant)  $s \pm$  survives, but the second ( $d_{x^2-y^2}$ ) insta-



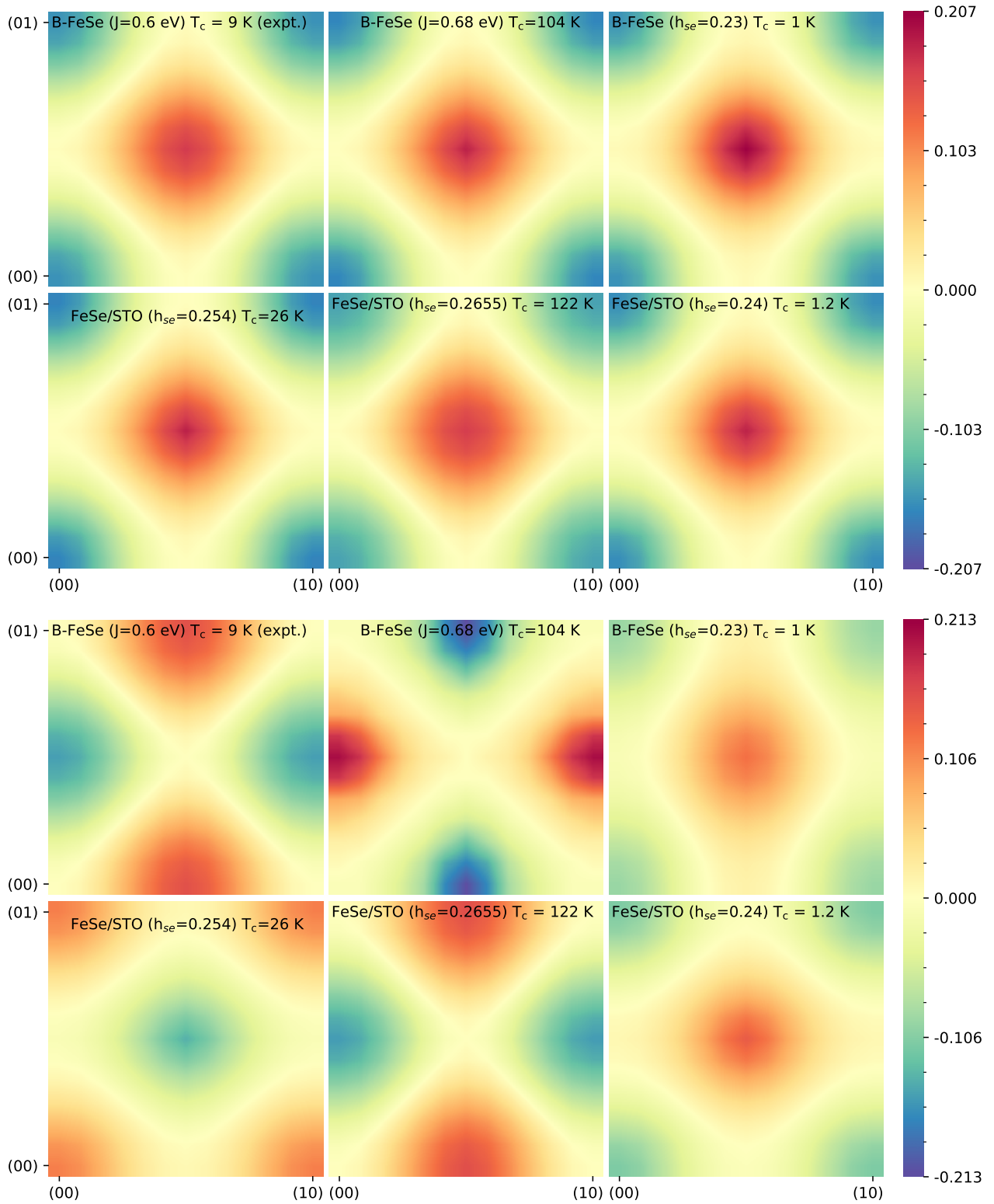


FIG. 3. The superconducting susceptibility, corresponding to the leading (top) and lagging (bottom) eigenvalues of the solutions to the linearized Eliashberg equations,  $\Delta(q, \omega = 0)$  are shown for bulk FeSe ( $J=0.6$  eV), bulk FeSe with increased Hund's correlation ( $J=0.68$  eV), reduced Fe-Se height ( $h_{Se}=0.23$ ), FeSe/STO<sup>48</sup>, FeSe/STO with  $h_{Se}=0.2655$  and  $h_{Se}=0.24$ . The leading superconducting instability in all cases has extended s-wave character, while the lagging instability has  $d_{x^2-y^2}$  character only when the  $d_{xy}$  state contributes to the hole pockets.

bility gets suppressed. Whenever the  $d_{xy}$  state is pushed below  $E_F$  at  $\Gamma$  and yet continues to be present at the

electron pockets, the only surviving superconducting instability is the  $s\pm$  state, consistent with the earlier predictions<sup>31,32</sup>. The leading superconducting instability results in an estimated  $T_c=26$  K. We also find that the  $T_c$  is insensitive to  $J$ . This estimate is lower than  $T_c=80$  K observed for FeSe/STO. The origin of the discrepancy may be due to the fact that interface can have several other effects absent in the present electronic theory, the phonons and dipolar effects are also missing.

To confirm that  $T_c$  is sensitive to the position of  $d_{xy}$ , we recalculate QSGW bands, QSGW+DMFT self-energy,  $\chi$ , and the pairing susceptibility for a pair of geometries: one with  $h_{Se}$  smaller than the (calculated) equilibrium value ( $h_{Se}=0.254$ ) and the other larger. For  $h_{Se}=0.24$ , QSGW puts the  $d_{xy}$  state at  $E_F-130$  meV on the  $\Gamma$ -Z line (right panel, Fig. 4). At the DMFT level, we find the system to be a coherent good metal; quasi-particle weight ranging between 0.56 to 0.42 and small scattering rate, with an upper bound 38 meV.  $\text{Im}\chi(q, \omega)$  shows weaker spin fluctuation dominated by low-energy  $(1/2, 1/2)$  peak and  $T_c$  drops to 1.2 K. The superconducting instability has extended  $s\pm$  structure and loses the  $d_{x^2-y^2}$  instability, similar to the bulk when  $h_{Se}$  was reduced. Increasing  $h_{Se}$  has the opposite effect. At  $h_{Se}=0.2655$  (corresponding to the bulk value),  $T_c$  increases to 56 K; both  $s\pm$  and  $d_{x^2-y^2}$  instabilities are present. As in the bulk case,  $d_{xy}$  contributes to the hole pockets at the Fermi energy (the  $d_{xy}$  band sits at  $E_F+40$  meV at  $\Gamma$ ), and  $T_c$  becomes sensitive to  $J$  again. A slightly larger  $J$  ( $J=0.71$  eV) can drive  $T_c$  to as high as 122 K. The orbital-resolved quasi-particle weight varies between 0.24 and 0.38 and the single-particle scattering rate can be as large as 380 meV for  $d_{xy}$ . We also observe significantly enhanced spin fluctuations at  $(1/2, 1/2)$ . All observations suggest significant enhancement in correlation.

To summarize, evidence from several parametric studies of FeSe make a unified picture of the origins of superconductivity in FeSe. It is mainly of  $s\pm$  character and is caused by low-energy spin fluctuations concentrated in a region near the antiferromagnetic ordering vector. In FeSe such a condition can appear when the Fe  $d_{xy}$  orbital is auspiciously placed near the Fermi level and further, that the Hund's  $J$  is sufficiently large to induce a high degree of “bad metallic” behavior. Some of the markers of a “bad metal” are incoherence in the spectral function, small and orbital-dependent  $Z$  factors, and large, orbital-dependent scattering rates, which for FeSe are concentrated in the  $d_{xy}$  orbital. Various kinds of parameterizations, making small excursions in parameter space about the *ab initio* one-body Hamiltonian, enable us to isolate the role of specific orbitals in the single-particle band structure and also Hund's  $J$  driving incoherence.

Hund's coupling can be used as a parameter to tune  $T_c$ , raising the possibility to breach the frontier of  $T_c=100$  K in iron chalcogenides. A possible way to control  $J$  in real materials is to change the electron screening cloud. We presented one instance that induced a change (monolayer vs bulk). Controlling number of layers, applying pressure

to tune Fe-chalcogenide bond length, doping and intercalation are some other possibilities. At the same time it is important to realize it is necessary to control both the screening and specific features of the single-particle spectrum. One of the most promising directions for reaching an optimized  $T_c$  appears to be controlling number of layers and interfaces to simultaneously satisfy both the promising conditions: lesser electron screening leading to a larger Hund's correlation and  $d_{xy}$  surviving at the hole pockets at the Fermi level.

## ACKNOWLEDGMENTS

This work was supported by the Simons Many-Electron Collaboration. For computational resources, we were supported by PRACE supercomputing facility and STFC Scientific Computing Department's SCARF cluster.

## METHOD

We use our recently developed quasi-particle self consistent  $GW$  + dynamical mean field theory (QSGW+DMFT)<sup>21,38,39</sup>, as implemented in the all-electron Questaal package<sup>41,43</sup>. Paramagnetic DMFT is combined with nonmagnetic QSGW via local projectors of the Fe  $3d$  states on the Fe augmentation spheres to form the correlated subspace. We carried out the QSGW calculations in the tetragonal phases of bulk FeSe and FeSe/STO. DMFT provides a non-perturbative treatment of the local spin and charge fluctuations. We use an exact hybridization expansion solver, namely the continuous time Monte Carlo (CTQMC)<sup>54</sup>, to solve the correlated impurity problem.

The one-body part of QSGW is performed on a  $16 \times 16 \times 16$  k-mesh and charge has been converged up to  $10^{-6}$  accuracy, while the (relatively smooth) many-body static self-energy  $\Sigma^0(\mathbf{k})$  is constructed on a  $8 \times 8 \times 8$  k-mesh, extracted from the dynamical  $GW$   $\Sigma(\mathbf{k}, \omega)$ .  $\Sigma^0(\mathbf{k})$  is iterated until convergence (RMS change in  $\Sigma^0 < 10^{-5}$  Ry). For all relevant compounds  $U$ ,  $J$  are computed from our implementation of constrained RPA<sup>41</sup>, starting from all electron QSGW band structure. The DMFT solution for the dynamical local self energy is iterated starting from the QSGW Hamiltonian; it converges in  $\approx 20$  iterations. Calculations for the single particle response functions are performed with  $10^9$  QMC steps per core and the statistics is averaged over 64 cores. The two particle Green's functions are sampled over a larger number of cores (40000-50000) to improve the statistics. We sample the local two-particle Green's functions with CTQMC for all the correlated orbitals and compute the local polarization bubble to solve the inverse Bethe-Salpeter equation (BSE) for the local irreducible vertex. Finally, we compute the non-local polarization bubble  $G(\mathbf{k}, \omega)G(\mathbf{k}-\mathbf{Q}, \omega-\Omega)$  and combined with the local irre-

ducible vertex<sup>21,39,43,44</sup> we obtain the full non-local spin and charge susceptibilities  $\chi^{s,c}(\mathbf{Q}, \Omega)$ . The susceptibilities are computed on a  $16 \times 16 \times 16$   $\mathbf{Q}$ -mesh. BSE equations in the particle-particle pairing channels are solved on the same  $\mathbf{k}$ -mesh to extract the susceptibilities and the linearised Eliashberg gap equations are solved to extract the eigenvalue spectrum and corresponding pairing instabilities<sup>21,44</sup>.

## ADDITIONAL INFORMATION

Supplementary material is available.

## CORRESPONDENCE

All correspondence, code and data requests should be made to SA.

- 
- \* swagata.acharya@kcl.ac.uk
- <sup>1</sup> Q. Si, R. Yu, and E. Abrahams, *Nature Reviews Materials* **1**, 16017 (2016).
  - <sup>2</sup> D.-H. Lee, *Annual Review of Condensed Matter Physics* **9**, 261 (2018), <https://doi.org/10.1146/annurev-conmatphys-033117-053942>.
  - <sup>3</sup> H. Luetkens, H.-H. Klauss, M. Kraken, F. Litterst, T. Dellmann, R. Klingeler, C. Hess, R. Khasanov, A. Amato, C. Baines, *et al.*, *Nature materials* **8**, 305 (2009).
  - <sup>4</sup> G. Aeppli, T. Mason, S. Hayden, H. Mook, and J. Kulda, *Science* **278**, 1432 (1997).
  - <sup>5</sup> D. Van Der Marel, H. Molegraaf, J. Zaanen, Z. Nussinov, F. Carbone, A. Damascelli, H. Eisaki, M. Greven, P. Kes, and M. Li, *Nature* **425**, 271 (2003).
  - <sup>6</sup> M. Civelli, arXiv preprint [arXiv:0710.2802](https://arxiv.org/abs/0710.2802) (2007).
  - <sup>7</sup> K. Haule, J. H. Shim, and G. Kotliar, *Phys. Rev. Lett.* **100**, 226402 (2008).
  - <sup>8</sup> A. Liebsch and H. Ishida, *Phys. Rev. B* **82**, 155106 (2010).
  - <sup>9</sup> H. Ishida and A. Liebsch, *Phys. Rev. B* **81**, 054513 (2010).
  - <sup>10</sup> M. Aichhorn, S. Biermann, T. Miyake, A. Georges, and M. Imada, *Phys. Rev. B* **82**, 064504 (2010).
  - <sup>11</sup> P. Werner, M. Casula, T. Miyake, F. Aryasetiawan, A. J. Millis, and S. Biermann, *Nature Physics* **8**, 331 (2012).
  - <sup>12</sup> A. A. Schafgans, S. J. Moon, B. C. Pursley, A. D. LaForge, M. M. Qazilbash, A. S. Sefat, D. Mandrus, K. Haule, G. Kotliar, and D. N. Basov, *Phys. Rev. Lett.* **108**, 147002 (2012).
  - <sup>13</sup> J. Fink, A. Charnukha, E. D. L. Rienks, Z. H. Liu, S. Thirupathiah, I. Avigo, F. Roth, H. S. Jeevan, P. Gegenwart, M. Roslova, I. Morozov, S. Wurmehl, U. Bovensiepen, S. Borisenko, M. Vojta, and B. Büchner, *Phys. Rev. B* **92**, 201106 (2015).
  - <sup>14</sup> M. Yi, Z. Liu, Y. Zhang, R. Yu, J.-X. Zhu, J. Lee, R. Moore, F. Schmitt, W. Li, S. Riggs, *et al.*, *Nature communications* **6**, 7777 (2015).
  - <sup>15</sup> H. Gretarsson, A. Lupascu, J. Kim, D. Casa, T. Gog, W. Wu, S. R. Julian, Z. J. Xu, J. S. Wen, G. D. Gu, R. H. Yuan, Z. G. Chen, N.-L. Wang, S. Khim, K. H. Kim, M. Ishikado, I. Jarrige, S. Shamoto, J.-H. Chu, I. R. Fisher, and Y.-J. Kim, *Phys. Rev. B* **84**, 100509 (2011).
  - <sup>16</sup> J. Pellicciari, Y. Huang, K. Ishii, C. Zhang, P. Dai, G. F. Chen, L. Xing, X. Wang, C. Jin, H. Ding, *et al.*, *Scientific reports* **7**, 8003 (2017).
  - <sup>17</sup> A. Georges, L. d. Medici, and J. Mravlje, *Annual Review of Condensed Matter Physics* **4**, 137 (2013), <https://doi.org/10.1146/annurev-conmatphys-020911-125045>.
  - <sup>18</sup> L. de' Medici, J. Mravlje, and A. Georges, *Phys. Rev. Lett.* **107**, 256401 (2011).
  - <sup>19</sup> L. Fanfarillo and E. Bascones, *Phys. Rev. B* **92**, 075136 (2015).
  - <sup>20</sup> K. Stadler, G. Kotliar, A. Weichselbaum, and J. von Delft, *Annals of Physics* **405**, 365 (2019).
  - <sup>21</sup> S. Acharya, D. Pashov, C. Weber, H. Park, L. Sponza, and M. van Schilfgaarde, arXiv preprint [arXiv:1811.05143](https://arxiv.org/abs/1811.05143) (2018).
  - <sup>22</sup> S. Acharya, M. S. Laad, D. Dey, T. Maitra, and A. Taraphder, *Scientific Reports* **7**, 43033 (2017).
  - <sup>23</sup> S. Acharya, D. Dey, T. Maitra, and A. Taraphder, *Journal of Physics Communications* (2018).
  - <sup>24</sup> H. U. Strand, M. Zingl, N. Wentzell, O. Parcollet, and A. Georges, arXiv preprint [arXiv:1904.07324](https://arxiv.org/abs/1904.07324) (2019).
  - <sup>25</sup> A. Mackenzie, S. Julian, A. Diver, G. Lonzarich, N. Hussey, Y. Maeno, S. Nishizaki, and T. Fujita, *Physica C: Superconductivity* **263**, 510 (1996), proceedings of the International Symposium on Frontiers of High - Tc Superconductivity.
  - <sup>26</sup> Y. Maeno, K. Yoshida, H. Hashimoto, S. Nishizaki, S.-i. Ikeda, M. Nohara, T. Fujita, A. Mackenzie, N. Hussey, J. Bednorz, and F. Lichtenberg, *Journal of the Physical Society of Japan* **66**, 1405 (1997), <https://doi.org/10.1143/JPSJ.66.1405>.
  - <sup>27</sup> C. Bergemann, A. P. Mackenzie, S. R. Julian, D. Forsythe, and E. Ohmichi, *Advances in Physics* **52**, 639 (2003), <https://doi.org/10.1080/00018730310001621737>.
  - <sup>28</sup> D. Stricker, J. Mravlje, C. Berthod, R. Fittipaldi, A. Vecchione, A. Georges, and D. van der Marel, *Phys. Rev. Lett.* **113**, 087404 (2014).
  - <sup>29</sup> T. M. McQueen, A. J. Williams, P. W. Stephens, J. Tao, Y. Zhu, V. Ksenofontov, F. Casper, C. Felser, and R. J. Cava, *Phys. Rev. Lett.* **103**, 057002 (2009).
  - <sup>30</sup> A. Kostin, P. O. Sprau, A. Kreisel, Y. X. Chong, A. E. Böhrer, P. C. Canfield, P. J. Hirschfeld, B. M. Andersen, and J. S. Davis, *Nature materials*, 1 (2018).
  - <sup>31</sup> T. Hanaguri, S. Niihata, K. Kuroki, and H. Takagi, *Science* **328**, 474 (2010).
  - <sup>32</sup> B. Zeng, G. Mu, H. Luo, T. Xiang, I. Mazin, H. Yang, L. Shan, C. Ren, P. Dai, and H.-H. Wen, *Nature communications* **1**, 112 (2010).

variants	a (Å <sup>0</sup> )	c	$h_{Se}$	U	$J$
Bulk FeSe <sup>55</sup>	3.779	5.5111	0.2655	3.4	0.60
Bulk FeSe ( $h_{Se}=0.23$ )	do	do	0.23	3.9	0.71
FeSe/STO <sup>48</sup>	3.905	5.5111	0.254	3.6	0.68

TABLE I. Structural parameters, fractional chalcogen height  $h_{Se}$  and computed U,  $J$  for the correlated many body Hamiltonian from our QSGW+c-RPA implementation. References are from where the structural inputs for QSGW calculations are taken.

- <sup>33</sup> W. Qing-Yan, L. Zhi, Z. Wen-Hao, Z. Zuo-Cheng, Z. Jin-Song, L. Wei, D. Hao, O. Yun-Bo, D. Peng, C. Kai, *et al.*, Chinese Physics Letters **29**, 037402 (2012).
- <sup>34</sup> J.-F. Ge, Z.-L. Liu, C. Liu, C.-L. Gao, D. Qian, Q.-K. Xue, Y. Liu, and J.-F. Jia, Nature materials **14**, 285 (2015).
- <sup>35</sup> N. Lanata, H. U. Strand, G. Giovannetti, B. Hellsing, L. de'Medici, and M. Capone, Physical Review B **87**, 045122 (2013).
- <sup>36</sup> Z. Yin, K. Haule, and G. Kotliar, Nature materials **10**, 932 (2011).
- <sup>37</sup> T. Kotani, M. van Schilfgaarde, and S. V. Faleev, *Phys. Rev. B* **76**, 165106 (2007).
- <sup>38</sup> L. Sponza, P. Pisanti, A. Vishina, D. Pashov, C. Weber, M. van Schilfgaarde, S. Acharya, J. Vidal, and G. Kotliar, Phys. Rev. B **95**, 041112 (2017).
- <sup>39</sup> S. Acharya, C. Weber, E. Plekhanov, D. Pashov, A. Taraphder, and M. Van Schilfgaarde, *Phys. Rev. X* **8**, 021038 (2018).
- <sup>40</sup> J. Tomczak, P. Liu, A. Toschi, G. Kresse, and K. Held, The European Physical Journal Special Topics **226**, 2565 (2017).
- <sup>41</sup> D. Pashov, S. Acharya, L. W. Lambrecht, R. J. Jackson, K. Belashchenko, D. A. Chantis, F. Jamet, and M. Weber, van Schilfgaarde, arXiv preprint 1907.06021 (2019).
- <sup>42</sup> E. Şaşıoğlu, C. Friedrich, and S. Blügel, *Phys. Rev. B* **83**, 121101 (2011).
- <sup>43</sup> .
- <sup>44</sup> H. Park, *The study of two-particle response functions in strongly correlated electron systems within the dynamical mean field theory*, Ph.D. thesis, Rutgers University-Graduate School-New Brunswick (2011).
- <sup>45</sup> Z. Yin, K. Haule, and G. Kotliar, Nature Physics **10**, 845 (2014).
- <sup>46</sup> Q. Wang, Y. Shen, B. Pan, X. Zhang, K. Ikeuchi, K. Iida, A. Christianson, H. Walker, D. Adroja, M. Abdel-Hafiez, *et al.*, Nature communications **7**, 12182 (2016).
- <sup>47</sup> M. C. Rahn, R. A. Ewings, S. J. Sedlmaier, S. J. Clarke, and A. T. Boothroyd, *Phys. Rev. B* **91**, 180501 (2015).
- <sup>48</sup> S. Mandal, P. Zhang, S. Ismail-Beigi, and K. Haule, *Phys. Rev. Lett.* **119**, 067004 (2017).
- <sup>49</sup> Q. Han, H. T. Dang, and A. Millis, Physical Review B **93**, 155103 (2016).
- <sup>50</sup> N. Dasari, S. R. K. C. S. Yamijala, M. Jain, T. S. Dasgupta, J. Moreno, M. Jarrell, and N. S. Vidhyadhiraja, *Phys. Rev. B* **94**, 085143 (2016).
- <sup>51</sup> E. M. Nica, R. Yu, and Q. Si, npj Quantum Materials **2**, 24 (2017).
- <sup>52</sup> J. W. Lynn and P. Dai, Physica C: Superconductivity **469**, 469 (2009).
- <sup>53</sup> K. Haule and G. L. Pascut, *Phys. Rev. B* **94**, 195146 (2016).
- <sup>54</sup> K. Haule, *Phys. Rev. B* **75**, 155113 (2007).
- <sup>55</sup> R. S. Kumar, Y. Zhang, S. Sinogeikin, Y. Xiao, S. Kumar, P. Chow, A. L. Cornelius, and C. Chen, The Journal of Physical Chemistry B **114**, 12597 (2010).

## I. SUPPLEMENTAL MATERIAL

Structural inputs for our calculations, low energy fitting procedure and parameters extracted from DMFT self energy, the method for extraction of superconducting  $T_c$ , superconducting eigenvalue corresponding to the leading instability and QSGW band structure for different variants of bulk, doped and FeSe/STO are presented. All DMFT and DMFT+BSE results presented in the main text is performed at 290 K. However, to extract  $T_c$  from the temperature dependence of leading eigenvalue,  $\lambda(T)$  of gap equation, for all cases, DMFT and DMFT+BSE calculations are performed between 580 K and 116 K.



variants	0	0.5	0.6	0.62	0.64	0.66	0.68	0.7	0.8	1.0
B-FeSe ( $h_{Se}=0.2655$ )	0.003	0.013	0.067	0.095	0.103	0.43	0.9	0.56	0.41	0.29
B-FeSe ( $h_{Se}=0.23$ )			0.003				0.004			
B-FeSe ( $h_{Se}=0.24$ )			0.007				0.007			
B-FeSe ( $h_{Se}=0.25$ )			0.01				0.014			
B-FeSe ( $h_{Se}=0.26$ )			0.016				0.04			
FeSe/STO ( $h_{Se}=0.254$ )			0.25				0.265	0.265		
FeSe/STO ( $h_{Se}=0.24$ )							0.014	0.014		
FeSe/STO ( $h_{Se}=0.2655$ )							0.56	0.9		

TABLE II. The leading superconducting eigenvalue from the solution of linearized Eliashberg equations for all compounds and excursion in  $J$  (in eV) and for different  $h_{Se}$ . For both and monolayer FeSe/STO once the  $h_{Se}$  is such that the  $d_{xy}$  state contributes the hole pockets at Fermi level, the superconducting eigenvalue becomes sensitive to Hund's coupling  $J$  and increases with increasing  $J$ .

variants	$\Gamma_{x^2-y^2}$	$z_{x^2-y^2}$	$\Gamma_{xz,yz}$	$z_{xz,yz}$	$\Gamma_{z^2}$	$z_{z^2}$	$\Gamma_{xy}$	$z_{xy}$
FeSe ( $h_{Se}=0.23$ )	0.018	0.74	0.022	0.69	0.020	0.68	0.034	0.61
FeSe/STO ( $h_{Se}=0.254$ )	0.022	0.39	0.028	0.31	0.018	0.34	0.17	0.28
FeSe/STO ( $h_{Se}=0.24$ )	0.01	0.56	0.016	0.45	0.01	0.52	0.038	0.42
FeSe/STO ( $h_{Se}=0.2655$ , $J=0.71$ eV)	0.08	0.38	0.139	0.27	0.089	0.3	0.38	0.24

TABLE III. Quasi-particle renormalization factor  $Z$ , single-particle scattering rate  $\Gamma$  for bulk FeSe with smaller  $h_{Se}$  ( $h_{Se}=0.23$ ) and FeSe/STO and different choices of  $h_{Se}$ .

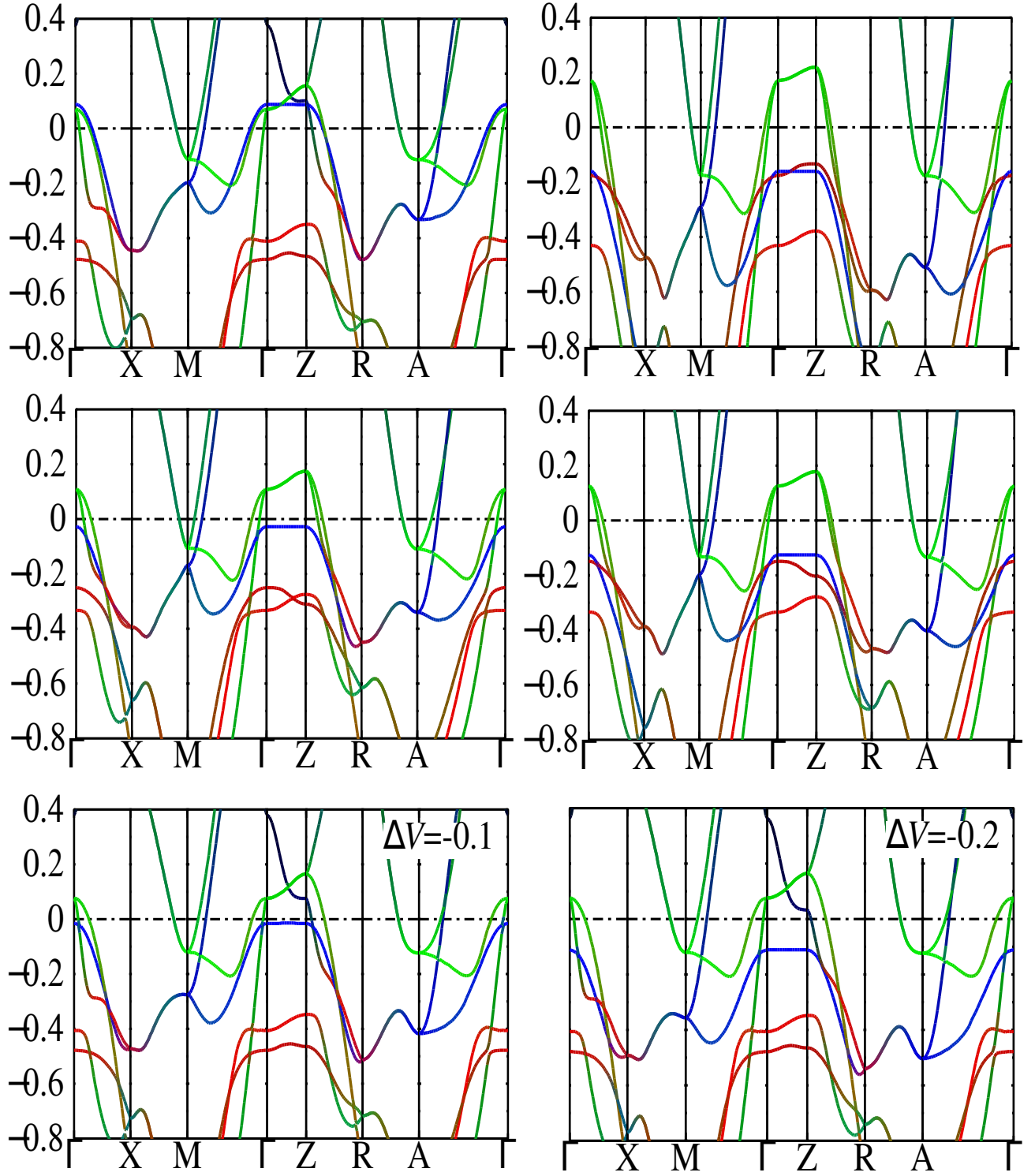


FIG. 4. Color weighted QSGW band structure plotted in the range of 0.4 eV above the Fermi energy and 0.8 eV below the Fermi energy. Top and middle rows correspond to left and right panels in Figs. 1 and 2 (crystalline FeSe on top, monolayer FeSe in the middle). Left panel is for  $h_{Se}$  at its equilibrium value (0.2655 in the crystalline case, 0.254 in the monolayer); right is for  $h_{Se}=0.23$  in the crystalline case and  $h_{Se}=0.24$  in the monolayer. Red, green and blue colors show projections onto Fe  $e_g$ ,  $d_{xz}+d_{yz}$ , and  $d_{xy}$  orbital characters, respectively. Bottom panels show QSGW band structure when modified by a combination of  $U$  added to the QSGW Hamiltonian combined with a constant background charged added to preserve the position of  $E_F$ , as discussed in the text. Note the close similarity with the top left panel, except for the shift in the  $d_{xy}$  (blue) band. Left panel: potential shift is  $\Delta V=nU=-0.1$  eV. Right panel: potential shift is  $\Delta V=nU=-0.2$  eV.

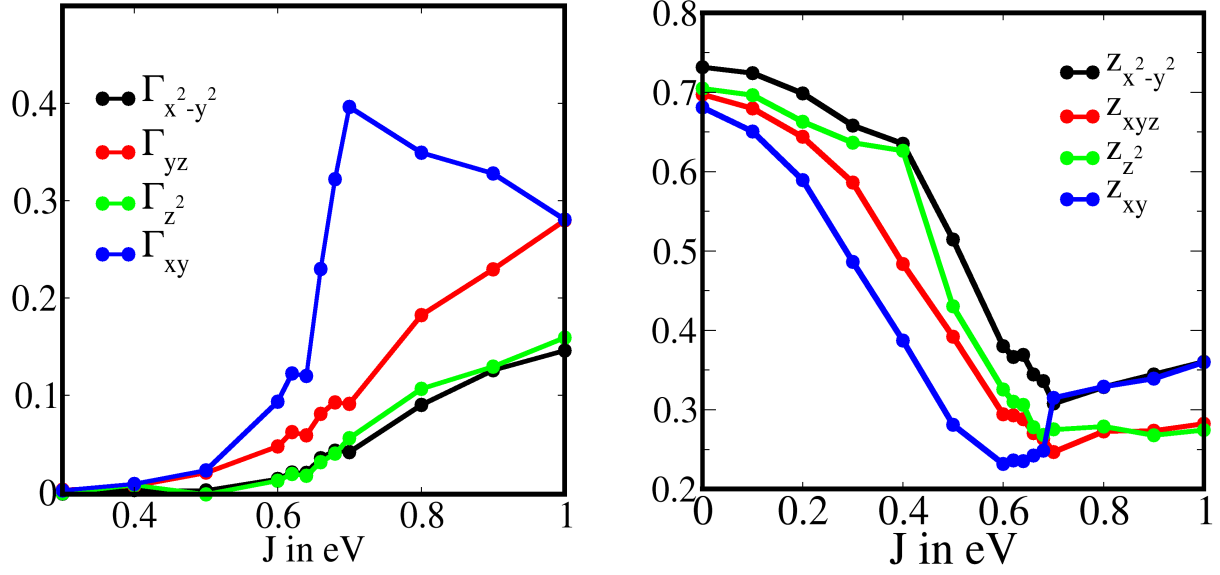


FIG. 5. Orbitaly resolved single-particle scattering rate ( $\Gamma$ ) and quasi-particle renormalization ( $Z$ ) factor for Bulk FeSe with varying Hund's coupling strength.  $\text{Im}\Sigma(i\omega)$  is fitted to a fourth order polynomial in  $i\omega$ . The mass enhancement, related to the coefficient ( $s_1$ ) of the linear term in the expansion  $m^*/m = 1 + |s_1|$ <sup>49</sup>, and the intercept  $|s_0| = \Gamma m^*/m$

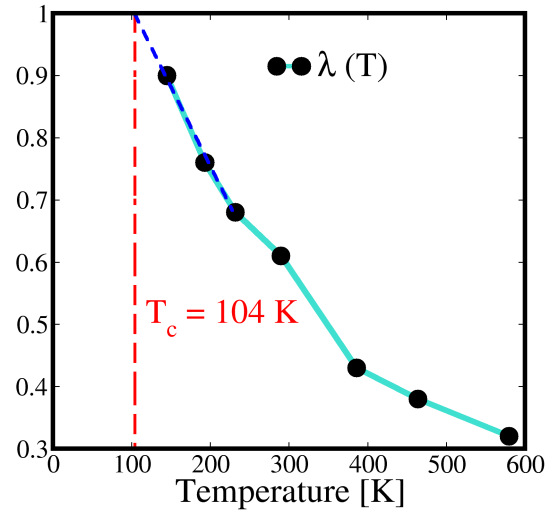


FIG. 6. Temperature dependence of the leading eigenvalue of the linearized Eliashberg gap equation solved in normal phase of FeSe bulk ( $J=0.68$  eV). The p-p pairing susceptibility diverges when the leading eigenvalue  $\lambda$  approaches one. The  $T_c$  for all the compounds are extracted in a similar fashion.